NANO-MICRO LETTERS

Vol. 2, No. 2
74-82 (2010)

Identification of binding interactions between myeloperoxidase and its antibody using SERS

E. S. Papazoglou*, S. Babu, S. Mohapatra, D. R. Hansberry and C. Patel

Surface Enhanced Raman Spectroscopy (SERS) is a widely used spectroscopic method that can dramatically increase the sensitivity of Raman spectroscopy and has demonstrated significant benefit in the identification of biological molecules. We report the use of SERS in differentiating the bound immunocomplex of myeloperoxidase (MPO) and its antibody from the unbound complex and its individual components. The SERS signal was enabled by gold nanoparticles attached to MPO, pAb and their immunocomplex at an excitation wavelength of 785 nm. The obtained SERS spectrum of MPO is in agreement with previous literature. Comparative SERS spectrum analysis of MPO, pAb, and their immunocomplex reveals the significant peak shifts and intensity variations caused by the conformational changes due to the immunocomplex formation. Several key areas have been identified which correspond to specific amino acids being shielded from undergoing resonance while new amino acid residues are made visible in the SERS spectrum of the immunocomplex and could be a result of conformational binding. Our work demonstrates the capability of SERS to identify binding events and differentiate an immunocomplex from its unbound components with direct applications in biosensors.

Keywords: Gold nanoparticle; Antigen; Immunocomplex; Biosensors

Citation: E. S. Papazoglou, S. Babu, S. Mohapatra, D. R. Hansberry and C. Patel, "Identification of binding interactions between myeloperoxidase and its antibody using SERS", Nano-Micro Lett. 2, 74-81 (2010). doi:10.5101/nml.v2i2.p74-82

Raman spectroscopy is a useful technique, based on Raman scattering, that has been widely used for molecular material characterization. When the electric field of a monochromatic light source (laser) interacts with a molecule it induces a dipole moment and causes the molecule to deform. The oscillatory nature of the laser beam's electric field causes periodic changes in the dipole moment resulting in vibration of the molecule which are characteristic of the molecule under investigation. The interaction of the molecule with a photon results in the molecule, either losing one vibrational quantum of energy or gaining one vibrational quantum of energy, and this is referred to as Stokes Raman scattering or anti-Stokes Raman scattering, respectively. Raman spectroscopy most commonly measures vibrational energy states but can also measure rotational or electronic energy states. The main challenge of Raman spectroscopy has been the difficulty in separating the weak inelastic Raman scattering signal from the overwhelmingly dominant elastic Rayleigh scattering. For every photon that undergoes Raman scattering there are at least 10 million photons that undergo Rayleigh scattering.

Surface-enhanced Raman spectroscopy (SERS) provides a solution to this challenge by enhancing the signal intensity of Raman scattering of molecules adsorbed to roughened metal surfaces by as much as 10^{15} [1]. Fleischman et al. [2] was the first to note this enhanced effect in 1973 while observing the adsorption of pyridine on a silver electrode. Later two groups,

School of Biomedical Engineering, Science & Health Systems, Drexel University, 3141 Chestnut Street, Pennsylvania 19104, Philadelphia
*Corresponding author. Email: esp25@drexel.edu, Telephone: 215-895-4956, Fax: 215-895-4983

Jeanmarie et al. [3] and Albrecht et al. [4] independently realized this as a unique phenomenon and proposed both an electromagnetic mechanism and a chemical mechanism, as theoretical explanations for the enhanced signal. Gold and silver nanoparticles are commonly used as SERS substrates with gold particles being used more frequently due to their high sensitivity and stability compared to silver compounds [5-8]. It must be noted that the enhanced Raman signal enabled by the plasmon resonance of gold and silver nanoparticles gave rise to new biosensors that have been used for identifying the binding region in proteins [9], and for studying binding affinity of immunoreactions [10]. Signal analysis of SERS was used to identify the native constituents of live epithelial cells employing endocytosed 60 nm gold nanoparticles [11]. SERS has also been used to differentiate bacteria from bacteriophages by conjugating them to 60nm gold nanoparticles [12] and in single molecule detection [13,14]. The combination of plasmon resonance based sensing with real-time SERS analysis could become a novel tool for interrogating the dynamics of protein binding interactions.

Applications of SERS in immunosensing include the successful detection of the thyroid stimulating hormone (TSH) [15], monitoring the immunocomplex formation between mouse IgG and goat anti-mouse IgG [16], detection of membrane bound enzymes within cells and correlation of prostaglandin-H-synthase (PGHS) antigen levels [17], and detection of conformational binding of anti-mouse IgG (bound to gold nanoparticles of 29.7 nm diameter) to mouse IgG antigen [18].

Myeloperoxidase (MPO) is a lysosomal protein found in neutrophilic granulocytes, often overexpressed in inflammatory diseases [19-21]. MPO is a vital protein found in neutrophilic granulocytes that has an instrumental role in attacking bacteria and foreign pathogens. Neutrophilic granulocytes phagocytose pathogens and eliminate them through chemical reactions. MPO is capable of producing both hypochlorous acid and tyrosyl radicals in independent pathways. Hypochlorous acid and the tyrosyl radical are both cytotoxic and degrade bacteria and foreign pathogens. MPO is a 140kDa dimmer composed of two identical halves, each with a covalently bound heme and connected by a lone disulfide bond. In addition to the heme group located on each half of the MPO molecule there is a bound calcium ion and three Asn-linked glycosylations (at Asn189, Asn225, Asn317) [22]. Sibbet et al. [23] examined the structure of canine MPO using resonance Raman spectroscopy and concluded that MPO contains two equivalent chlorine prosthetic groups.

To our knowledge Raman spectroscopic studies on MPO have been primarily performed using Resonance Raman Spectroscopy (RRS). RRS yields higher peak intensity compared to conventional Raman spectroscopy which translates to a lower sample concentration requirement. Our interest lies in using SERS to identify bands that are unique to the immunocomplex of MPO and its antibody and explore the use of such bands as signatures of binding events. In this paper, we report our results in differentiating the SERS signal of the MPO/pAb immunocomplex from the unbound complex and its individual components.

EXPERIMENTAL METHODS

All chemicals were purchased from Sigma Aldrich unless otherwise mentioned, pAb (rabbit anti human myeloperoxidase) was purchased from ABD-Serotec and myeloperoxidase (MPO) was purchased from Lee Biosolutions Inc.

Gold nanoparticles were prepared according to Frens, G. [24] with added modifications. 500µl of 1% chloroauric acid ($HAuCl_4$) were added to 50ml of distilled H_2O and heated to a boil under constant stirring. Upon boiling 400µl of 1% citric acid ($C_6H_8O_7$) were added. The size of nanoparticles could be controlled by varying the volume of citric acid being added; higher volume corresponds to smaller particles and lower volume corresponds to larger particles. 400µl of 1% citric acid correspond to 40nm particles. The solution was refluxed until the color was changed from dark blue to red. The solution was then removed from heat and allowed to cool to room temperature. The solution was further dialyzed in DI H_2O for 48 hours with the water being changed at 3, 12, and 24 hours, in order to remove citrate ions from the solution. Particle characterization was performed with UV-vis spectroscopy [25], atomic force microscopy, and scanning electron microscopy. Thus prepared gold nanoparticles were then immobilized on silane functionalized glass slides. Silanization of glass slides was achieved by the method followed by Park et al. [26]. In brief, glass slides were cleaned using piranha solution (1:3 v/v, H_2O_2:H_2SO_4) and dried under nitrogen. Cleaned glass slides were then immersed in 3% 3-aminopropyltrimethoxysilane (APTMS) in methanol for 3 hours. Silanized slides were then rinsed thoroughly with methanol followed by DI water and drying with a jet of dry nitrogen. Silanized glass slides were then immersed in the dialyzed gold nanoparticle solution for 3 hours. Slides with immobilized gold nanoparticles were then washed with DI water and air dried. A well with a capacity of ~100 mL was constructed using plastic pipette and epoxy on top of the glass slide to facilitate pAb immobilization and subsequent SERS data collection.

Polyclonal antibody was immobilized by letting ~100 ml of 100 nM pAb solutions interact with the gold nanoparticle coated slides for 15 minutes at room temperature followed by thorough washing with 1x PBS buffer (pH7.4). Gold nanoparticles coated with pAb were then allowed to interact with MPO (100 µl, 1 µM) for 15 minutes at room temperature followed by washing. A similar procedure was followed to immobilize MPO (100 µl, 1 M) directly on gold nanoparticles. SERS data was collected from the Au-pAb conjugates, Au-pAb/MPO immunocomplex, and Au-MPO conjugates immediately after preparation using a Renishaw RM1000 confocal Raman microspectrometer with a 50x long focal microscope. A 785nm diode laser (15 mW) was used to collect the SERS signal. Care was taken to maintain a ~50 µl of PBS buffer to minimize thermal damage and the SERS data was collected from an area of ~40x40 µm square (~100 data points) located at the center of the well. SERS signal from glass slides coated with gold nanoparticles was also collected and served as the background signal.

Spectra with errors due to cosmic ray influence were removed manually resulting in an average of 75 spectra per sample. Individual spectra were then subjected to a three point baseline correction. The three points for baseline correction were kept the same for all spectra and samples, typically the first and last point corresponding to the beginning and end of the wave numbers of the spectra and the third point being set at 1369 cm^{-1}. This baseline correction applied to all data sets helped smooth the data and allow an appropriate comparison. Following the baseline correction individual spectra were normalized and averaged. In order to remove the gold nanoparticle (AuNp) signature from the spectra, the average AuNp spectrum set was subtracted from averaged spectra of Ab, MPO and MPO-pAb. The sum of Ab and MPO spectra was obtained by simply averaging the two spectra in Origin Pro. Origin 8.0's peak analyzer module was used to fit peaks to the averaged spectra.

RESULTS AND DISCUSSION

Raw SERS spectra of AuNp, Ab, MPO, and MPO-pAb are shown in Fig. 1a-1d, respectively. Individual spectra in Fig. 1 were sorted by their average intensity for easy visualization. The background spectra i.e. spectra of AuNp (see Fig. 1a) reveal the typical fluorescence response of AuNp under experimental conditions [27]. Peak positions as well as peak width remain the same between various spots on the scanned area, demonstrating the reproducibility of the collected SERS data. Figure 1b-1d demonstrate the influence of the AuNp on the spectra of the pAb, MPO and MPO-pAb respectively. This necessitates removal of the AuNp interference from the rest of the dataset. Baseline corrected Ab, MPO and MPO-pAb spectra are shown in Fig. 2a, b and c, respectively. In order to identify spectral changes due to the binding of pAb and MPO as opposed to simple superposition

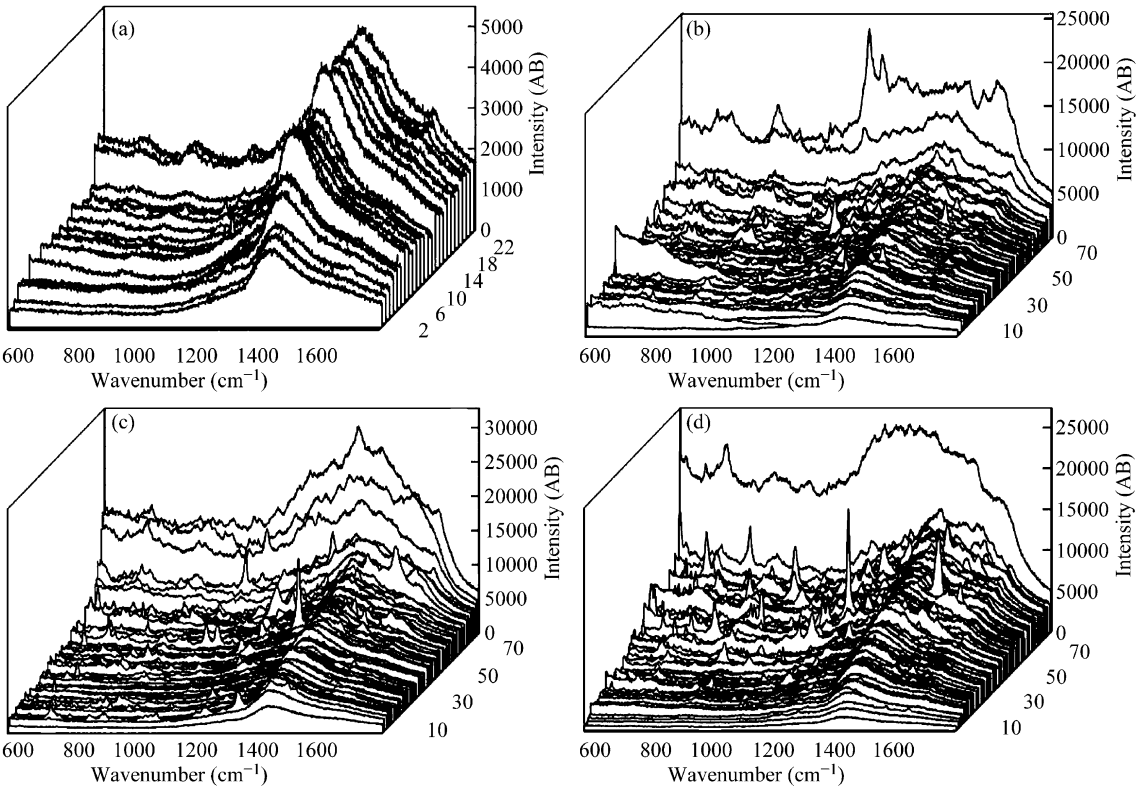

FIG. 1. Raw SERS spectra of (a) Gold nanoparticles, (b) polyclonal antibody, (c) myeloperoxidase and (d) immunocomplex.

we compared the spectra of AbMPO and the sum of spectra of pAb and MPO as shown in Fig. 3. Table 2 the peak positions of AbMPO along with the peaks that were found to be distinct for their immunocomplex. The peak positions that are unique for the immunocomplex are shown with the respective error bars (average of 80 spectra).

The SERS spectrum of MPO (see Fig. 2b) exhibits strong similarities to the Raman signals reported in previous studies [23,28-31]. It is relatively weak below 1100 cm^{-1}, besides three small peaks between 646 cm^{-1} (ν_{48}/ν_{25}) to 684 cm^{-1}(ν_7), at 835 cm^{-1}, and between 992 cm^{-1}(γ(CH)) and 1007 cm^{-1}(ν_{45}). Table 1 summarizes the MPO Raman peaks published by various studies. The minor peak assignments in our study are in excellent agreement with Zbylut S. D. et al., including the vibrational modes at ν_{45} (1007 cm^{-1}), γ(CH) (992 cm^{-1}), ν_{46} (925 cm^{-1}), γ_{10} (853 cm^{-1}), γ_{15} (710 cm^{-1}), ν_7 (684 cm^{-1}), and ν_{48}/ν_{25} (646 cm^{-1}) [32]. The MPO spectrum from 1120 cm^{-1} to 1260 cm^{-1} is also found to be similar to that previously published from resonance Raman spectra [31]. Notably there are significant peaks at 1137 cm^{-1}(ν_{44}), 1214 cm^{-1}(ν_{13}), and 1251 cm^{-1}(ν_{42}). These peaks are consistent with previous literature on resonance Raman spectra of MPO [23,28-31]. Our work using a 785 nm excitation

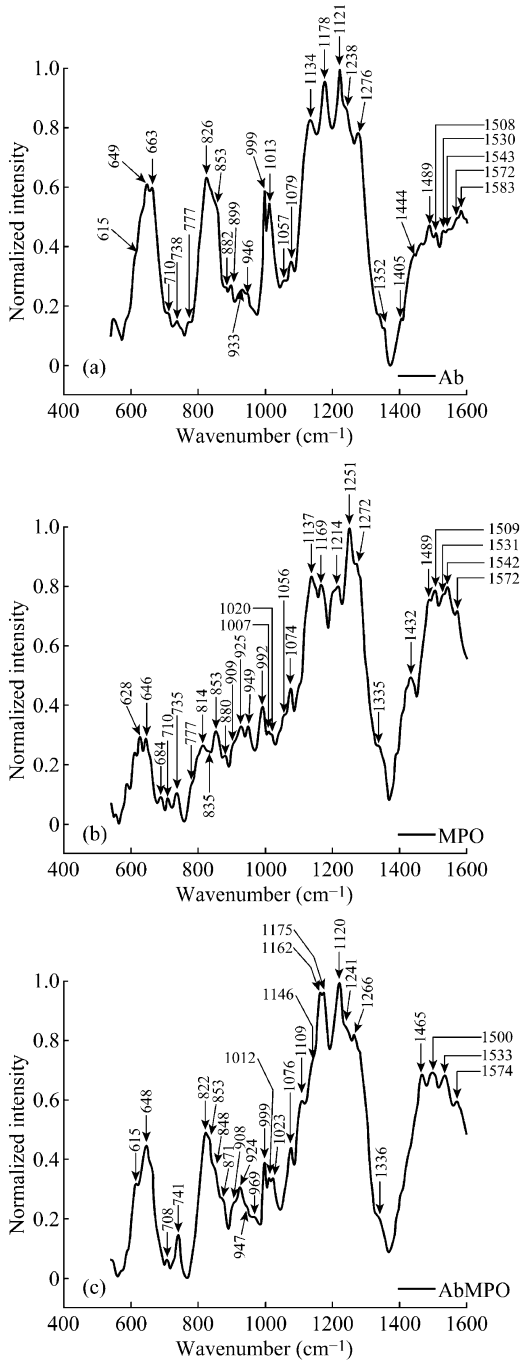

FIG. 2. SERS spectra of averaged (a) Ab, (b) MPO, and (c) AbMPO

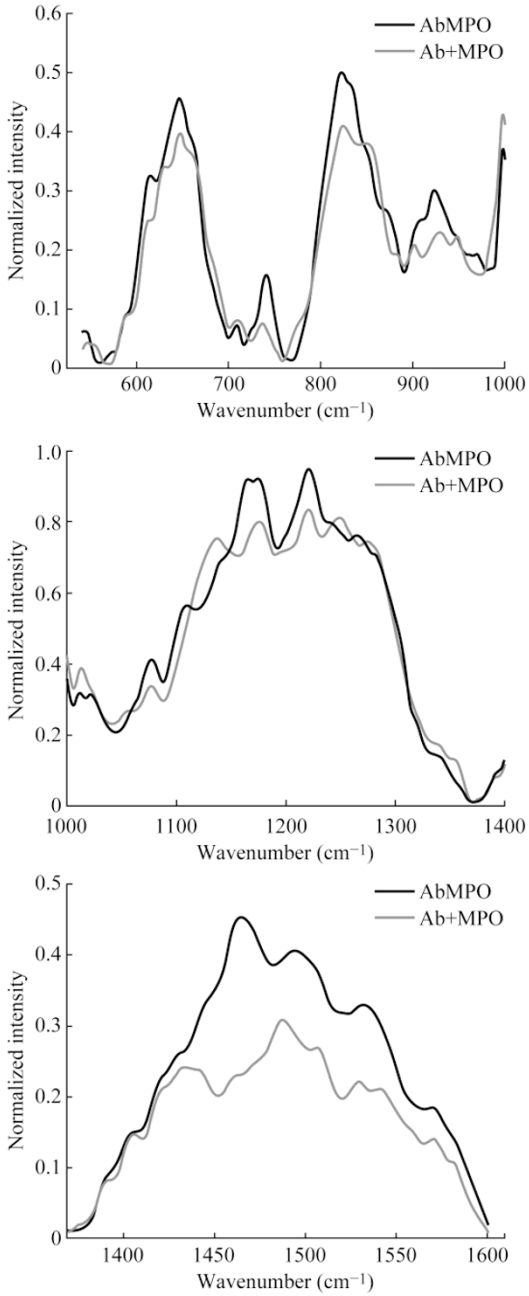

FIG. 3. Comparison of AbMPO spectra with sum of Ab and MPO spectra.

Table 1. Comparison of MPO Raman signal across multiple studies.

vibrational mode	sym. species	MPO^{3+} a	MPO^{3+} b	MPO^{2+} b	MPO^{3+} c	MPO^{2+} c	MPO^{3+} d	MPO^{2+} d	MPO^{3+} e	MPO^{3+} f	MPO^{3+} g	MPO^{3+} h	MPO^{2+} h
v10	*B1g*	–	1620 s	1608 s	1617	–	–	–	–	–	–	–	–
ν (C=C)	–	–	1615 s	overlapped	–	1607	1614	1606	1614	1612	1614	1610	1607
v37	*Eu*	–	1595j,k m	–	1588	–	1592	1582	–	—	1593	–	–
v2	*A1g*	–	1590 s	1588 s	1568	1587	–	–	1585	1587	1576	1585	1586
v19	*A2g*	1572	1569 m	1564i	–	1561	–	–	–	–	–	–	–
v11	*B1g*	–	1552 s	1548 m	1551	1544	–	–	–	1550	1543	1550	1549
–	–	–	1545j	–	–	–	1552	1545	–	–	–	–	–
v38	*Eu*	1531	1525 m	1527i	1523	1524	1523	1523	–	1523	–	1524	1528
2v15	–	1509	1505j	–	–	–	–	–	–	–	1504	–	–
v3	*A1g*	1488	1483 m	1470 m	1482	–	1486	1472	–	1479	1481	1481	–
v28	*B2g*	–	1474 l	–	–	1469	–	–	1472	–	–	–	1472
δ (=CH2)	–	1432	1430 w	1425 w	–	1422	–	1424	–	–	–	–	1424
v40	*Eu*	–	1396 sh	1401 sh	–	1396	–	–	–	–	–	–	–
v20	*A2g*	–	1387 l	1379 w	1378	–	–	–	–	–	1386	–	–
v12	*B1g*	–	1375 s	1362 sh	–	1378	–	–	–	1377	–	1376	1377
v4	*A1g*	–	1366 s	1352 s	1366	–	1366	1359	–	–	–	–	–
2v7	–	–	1362j	–	–	1351	–	–	1359	1363	1363	1362	1355
v41	*Eu*	1335	1335 m	1331 w	1339	1329	–	–	–	–	1332	1331	–
δ (CH=)	–	–	1326 sh	1320 sh	–	–	–	–	–	–	–	–	–
v21	*A2g*	–	1305 m	1305 w	1307	1306	–	–	–	1307	1307	1306	–
CH2 wag	–	1272	1268 m	1267 m	1267	1267	–	–	–	–	–	1265	1265
v42	*Eu*	1251	1248 w	1242 m	–	1241	–	–	–	–	1238	1240	1242
CH2 twist	–	–	1223 w	–	–	–	–	–	–	–	–	–	–
v13	*B1g*	1214	1205 m	1205 m	1207	1206	–	–	–	1206	1208	1205	1207
v30	*B2g*	1169	1173 vw	1156 vw	1161	–	–	–	–	–	–	1163	1162
v44	*Eu*	–	1142k	–	–	1139	1116	1116	–	–	–	–	–
v14	*B1g*	1137	1130 m	1137 w	1133	–	–	–	1131	1134	1130	1132	1138
v5/v22	*A1g/A2g*	–	1112 m	1107 m	1114	1107	–	–	–	1111	1111	1106	1107
δ $(=CH2)_{as}$	–	1073	1063 w	–	–	1068	–	–	–	–	–	1069	1068
v23	*A2g*	–	1033 w	1029 vw	1034	1026	–	–	–	–	1034	1029	1027
v45	*Eu*	1007	998 m	984 w	1003	–	–	–	–	1003	1001	1003	–
γ (CH)	–	992	985 w	984 w	979	989	–	–	–	–	984	–	983
v46	*Eu*	–	935 vw	–	934	–	–	–	–	–	–	–	–
γ $(–C_bH_2)_s$	–	925	–	–	–	925	–	–	–	–	–	–	–
γ 10	*B1u*	853	861 w	–	858	860	–	–	–	–	–	859	862
–	–	835	830 w	–	835	825	–	–	–	–	832	837	841
v47	*Eu*	–	770 sh	–	–	–	–	–	–	–	–	–	–

v15	*B*1*g*	–	757 m	750 m	757	748	–	–	748	757	757	749	749
γ 11	*B*1*u*	710	717 m	715 vw	–	717	–	–	–	–	–	715	715
γ 15	*B*2*u*	–	704 sh	703 sh	–	–	–	–	–	–	–	–	–
v7	*A*1*g*	684	675 m	675 m	676	675	676	676	676	675	–	675	676
v48/v25	*Eu*/*A*2*g*	646	562 w	–	–	–	–	–	–	–	–	557	–
γ 21	*Eg*	–	–	–	–	–	–	–	–	–	–	–	–
v49	*Eu*	–	523 sh	–	–	520	–	–	–	–	–	517	517
γ 12	*B*1*u*	–	506 m	–	–	–	–	–	–	–	–	–	–
v33	*B*2*g*	–	453 sh	–	443	–	–	–	–	–	–	–	–
γ 22	*Eg*	–	434 m	–	–	–	–	–	–	437	–	437	438
$\delta(C_\beta C_a C_b)$	–	–	410 s	403 vw	411	402	410	–	–	408	–	409	403
v8	*A*1*g*	–	340 sh	–	–	–	–	–	344	–	–	–	–
γ 6	*A*2*u*	–	328 m	325 vw	329	326	–	–	–	328	–	329	324
v17	*B*1*g*	–	313j	–	–	–	–	–	–	–	–	–	–

a, our data (excitation wavelength of 785 nm); b, from [35] with additions from [32] (excitation wavelength of 406.7 nm); c, from [28] (excitation wavelength of 457.9 nm); d, from [31] (excitation wavelength of 413.1 nm); e, from [31] (excitation wavelength of 413.1 nm); f, from [31] (excitation wavelength of 457.9 nm); g, from [29] (excitation wavelength of 660nm); h, from [23] (excitation wavelength of 454.5 nm); i, from [35], strong (excitation wavelength of 496.5 nm); j, from [35], observed or very strong in the spectrum (excitation wavelength of 568.2 nm); k, from [35], strong (excitation wavelength of 406.7 nm); l, from [35], strong (excitation wavelength of 514.5 nm); m, medium; s, strong; sh, sharp, w, weak; vw, very weak.

Table 2. Comparison of SERS peak positions

No	Ab	MPO	AbMPO immunocomplex	Ab + MPO	No	Ab	MPO	AbMPO immunocomplex	Ab + MPO
1	615		615		28			1109	
2		628			29	1134	1137		1135
3	649	646	648	649	30			1146	
4	663		661		31		1169	1162	
5		684			32	1178		1175	1175
6	710	710		712	33	1221	1214	1220	1218
7	738	735	741	735	34	1238			
8	776			779	35		1251		1248
9		814			36	1276	1272	1266	1275
10	826		822	824	37		1335		
11		835	835		38	1352			
12	853	853	848	855	39	1405			
13			871		40	1444			1442
14		880			41		1432		
15	882				42			1465	
16	899			902	43	1472			
17		925	924	925	44	1489	1488		1489
18	933				45			1500	
19	946	949		950	46	1508	1509		1508
20			969		47	1530	1531	1533	1532
21			984		48	1543			1543
22	999	992	999	993	49				1556
23		1007	1012	1011	50	1572	1572	1574	1573
24	1013				51	1583			
25		1020	1023		52	1608			1602
26	1057	1056		1064	53		1690		
27	1079	1074	1076						

used different excitation wavelengths (ranging from 406.7 nm to 660 nm) [23,28-31]. Therefore the results obtained suggest that the key identifying MPO peaks are independent of the excitation wavelength, or the Raman method (RRS, CARS or SERS) that was used to collect the data. It is encouraging to also see that the SERS spectrum of the pAb has characteristic peaks similar to previously obtained Raman signals of an IgG. This is not surprising given the structural similarities of the antibodies. The complete list of peaks from Fig. 2 is presented in Table 2.

Figure 2 compares the SERS spectra of MPO, pAb, and the immunocomplex of MPO bound to pAb and Table 2 lists and compares the peaks of each spectrum. Beginning at 500 cm^{-1} and working towards 1650 cm^{-1} we observe distinct peak shifts, altered intensities, and unique peaks when comparing MPO, pAb, and their immunocomplex. Signal intensity alone may not be sufficient to differentiate between bimolecular especially in the SERS mode (amplification factors and specific binding may alter the signal intensity significantly) [33]. It may rather be a combination of signal intensity and peak position that can provide a more reliable means for identifying a given sample. The differences shown in Fig. 2 suggest that the immunocomplex formation could result in changes in conformation, orientation of bonds, and changes in the functional groups within the plasmon resonance distance of thegold nanoparticle. New peaks at 871 cm^{-1}, 1109 cm^{-1}, and 1465 cm^{-1} present in the immunocomplex and not found in either MPO or pAb alone, indicate a tryptophan moiety made now visible in the SERS spectrum, possibly a result of conformational changes after binding. Furthermore, new peaks at 969 cm^{-1}, 984 cm^{-1}, 1146 cm^{-1} and 1500 cm^{-1} which are not found in the MPO or pAb signal, indicate the immunocomplex formation. In the Tyr and Amide III region, a peak shift in the pAb spectra from 1276 cm^{-1} to 1266 cm^{-1} in the immunocomplex may also correspond to conformational changes.

The critical element in claiming that SERS is capable of identifying binding between MPO and the pAb is the significant difference between a composite spectrum obtained by addition of MPO and pAb and the SERS of the immunocomplex. For the purpose of comparison we are including the spectra of the immunocomplex and the composite spectrum (i.e. sum of pAb and MPO) as normalized average (see Fig. 3). Figure 3 compares the composite and immunocomplex spectra, and for ease of visualization the spectra was divided into 3 sections and presented as Fig. 3a, b, and c. The ability to differentiate such subtle differences without extensive data analysis procedures demonstrates the simplicity of the approach and the sensitivity of the SERS method in differentiating the binding interactions of an immunocomplex from unbound antigen/antibody pair. Relative standard errors (RSE) calculated (n=80) at peak positions that are unique for the immunocomplex are shown in Table 3. RSE at the new peak positions varied significantly, with a minimum deviation (18%) at 1465 cm^{-1}. We attribute these variations to possible orientation differences of the Au particles. It is well established that the amplification factor of the SERS substrate largely depends on the crystal facets to which the molecules are absorbed. Recently Yu et al employed SERS for studying the effect of charge on the orientation of cytochrome c [34] and concluded that the molecules have random orientation on a bare Au nanohole surface. In the present study, it is highly probable that orientation and the crystal facet of the Au particles were totally random. Since the SERS data was collected over a large surface area compared to the size of a cluster of particles it would be important to identify the influence of the crystal orientation on the obtained SERS data, especially on the new peaks. We believe it is possible to minimize these variations by improving the homogeneity of the SERS substrate using the methods proposed by Liu et al [27].

Table 3. Relative standard error at peak positions identified as unique to immunocomplex.

Peak Position (cm^{-1})	Relative Standard Error (%)
870.6798	48.0
968.7625	48.0
1109.126	62.0
1145.536	51.0
1464.528	18.0
1500.479	30.0

CONCLUSIONS

Our results demonstrate that binding between an antigen (MPO) and its antibody gives rise to unique peaks absent in the compsoite spectra, derived by mere addition of the respective MPO and MPO-Ab Raman signatures. A valid question is how universal these peaks are and if one should expect to find identical or similar peaks upon binding of any antigen to its antibody. Data on the Raman of IgG antibodies have demonstrated that all IgG Raman spectra are very similar, while antigen Raman spectra depend on their particular structures. For classes of antigen / IgG antibodies where the binding interactions resemble the MPO/MPO-Ab binding, one would expect to find

similar peaks, possibly shifted but in the vicinity of the peaks we have identified. However, for binding pairs where the interaction sites are different chemical entities, totally different peaks would arise. A systematic study of such classes of antigen/Ab pairs would be very useful to create a library of practical significance to many scientific studies.

In summary, we investigated the potential application of SERS in differentiating the bound immunocomplex of an antigen and its antibody from the unbound complex and its components using myeloperoxidase as the model antigen. Obtained results indicate that the SERS spectrum of the immunocomplex is different from that of its parent antigen or antibody, and it is possible to identify conformational changes due to immunocomplex formation. Furthermore, the smallest RSE (18%, n=80) at 1465 cm^{-1} in the SERS spectra of the immunocomplex supports the notion that further investigation at this particular vibrational mode could provide valuable information towards application of SERS in understanding the changes that occur at a molecular level during binding interactions in biomolecules.

The authors wish to express their gratitude for the expert advice and training provided by Dr. Zhorro Nikolov, Director of the Centralized Research Facilities at Drexel University. This work was partially supported by the W. M. Keck Institute for Attofluidics at Drexel University.

Received 5 March 2010; accepted 30 March 2010; published online 27 April 2010.

References

1. S. Nie and S. R. Emory, Science 275, 1102 (1997). doi:10.1126/science.275.5303.1102
2. M. Fleischmann, P. J. Hendra and A. J. McQuillan, Chem. Phys. Lett. 26, 163 (1974). doi:10.1016/0009-2614(74)85388-1
3. D. L. Jeanmaire and R. P. Van Duyne, J. Electroanal. Chem. 84, 1 (1977). doi:10.1016/S0022-0728(77)80224-6
4. M. G. Albrecht and J. A. Creighton, J. Am. Chem. Soc. 99, 5215 (1977). doi:10.1021/ja00457a071
5. J. Hu, Z. Wang and J. Li, Sensors 7, 3299 (2007). doi:10.3390/s7123299
6. M. Suzuki, Y. Niidome, Y. Kuwahara, N. Terasaki, K. Inoue and S. Yamada, J. Phys. Chem. B 108, 11660 (2004). doi:10.1021/jp0490150
7. P. C. Lee and D. Meisel, J. Phys. Chem. 86, 3391 (1982). doi:10.1021/j100214a025
8. K. Kneipp, R. R. Dasari and Y. Wang, Appl. Spectrosc. 48, 951 (1994). doi:10.1366/0003702944029776
9. K. Stubenrauch, U. Wessels, R. Vogel and J. Schleypen, Analy. Biochem. 390, 189 (2009). doi:10.1016/j.ab.2009.04.021
10. H. W. Zhao, C. Z. Huang, L. P. Wu, S. F. Shen and Z. H. Qin, Anal. Lett. 42, 1495 (2009). doi:10.1080/00032710902961099
11. K. Kneipp, A. S. Haka, H. Kneipp, K. Badizadegan, N. Yoshizawa, C. Boone, K. E. Shafer-Peltier, J. T. Motz, R. R. Dasari and M. S. Feld, Appl. Spectrosc. 56, 150 (2002). doi:10.1366/0003702021954557
12. L. J. Goeller and M. R. Riley, Appl. Spectrosc. 61, 679 (2007). doi:10.1366/000370207781393217
13. A. K. Kalkan and S. J. Fonash, Appl. Phys. Lett. 89, 233103 (2006). doi:10.1063/1.2399369
14. E. J. Bjerneld, Z. Foldes-Papp, M. Kall and R. Rigler, The J. Phys. Chem. B 106, 1213 (2002). doi:10.1021/jp012268y
15. T. E. Rohr, T. Cotton, N. Fan and P. J. Tarcha, Anal. Biochem. 182, 388 (1989). doi:10.1016/0003-2697(89)90613-1
16. M. L. Zhang, C.Q. Yi, X. Fan, K. Q. Peng, N. B. Wong, M. S. Yang, R. Q. Zhang and S. T. Lee, Appl. Phys. lett. 92, 043116 (2008). doi:10.1063/1.2833695
17. S. R. Hawi, S. Rochanakij, F. Adar, W. B. Campbell and K. Nithipatikom, Anal. Biochem. 259, 212 (1998). doi:10.1006/abio.1998.2661
18. X. Dou, Y. Yamaguchi, H. Yamamoto, S. Doi and Y. Ozaki, J. Raman Spectrosc. 29, 739 (1998). doi:10.1002/(SICI)1097-4555(199808)29:8<739::AID-JRS289>3.0.CO;2-S
19. J. Merlie, D. Fagan, J. Mudd and P. Needleman, J. Biol. Chem. 263, 3550 (1988).
20. S. Kimura and M. Ikeda-Saito, Protein. Struct. Funct. Genet. 3, 113 (1988). doi:10.1002/prot. 340030206
21. P. M. Marie-Madeleine CALS, Ghislaine BRIGNON, Patricia ANGLADE and Bruno Ribadeau DUMAS, Eur. J. Biochem. 198, 733 (1991).
22. J. Zeng and R. E. Fenna, J. Molecular Bio. 226, 185 (1992). doi:10.1016/0022-2836(92)90133-5
23. S. S. Sibbett and J. K. Hurst, Biochem. 23, 3007 (1984). doi:10.1021/bi00308a025
24. G. Frens, Nature: Physical Science 241, 20 (1973).
25. W. Haiss, N. T. K. Thanh, J. Aveyard and D. G. Fernig, Anal. Chem. 79, 4215 (2007). doi:10.1021/ac07 02084
26. S. H. Park, J. H. Im, J. W. Im, B. H. Chun and J. H. Kim,

Microchemical Journal 63, 71 (1999). doi:10.1006/mchj.1999.1769

27. F. M. Liu and M. Green, J. Mater. Chem. 14, 1526 (2004). doi:10.1039/b400488b
28. G. T. Babcock, R. T. Ingle, W. A. Oertling, J. C. Davis, B. A. Averill, C. L. Hulse, D. J. Stufkens, B. G. J. M. Bolscher and R. Wever, BBA-Protein Struct. M. 828, 58 (1985).
29. G. J. Puppels, H. S. Garritsen, G. M. Segers-Nolten, F. F. de Mul and J. Greve, Biophys. J. 60, 1046 (1991). doi:10.1016/S0006-3495(91)82142-7
30. N. M. Sijtsema, Thesis, University of Twente, 1997.
31. C. Otto, N. M. Sijtsema and J. Greve, Eur. Biophys. J. 27, 582 (1998). doi:10.1007/s0024900 50169
32. S. D. Zbylut and J. R. Kincaid, J. Am. Chem. Soc. 124, 6751 (2002). doi:10.1021/ja01 2578u
33. A. M. Ahern and R. L. Garrell, Langmuir 7, 254 (1991). doi:10.1021/la00050a009
34. Q. M. Yu and G. Golden, Langmuir 23, 8659 (2007). doi:10.1021/la7007073
35. S. Brogioni, A. Feis, M. P. Marzocchi, M. Zederbauer, P. G. Furtmüller, C. Obinger and G. Smulevich, J. Raman Spectrosc. 37, 263 (2006) doi:10.1002/jrs.1442